

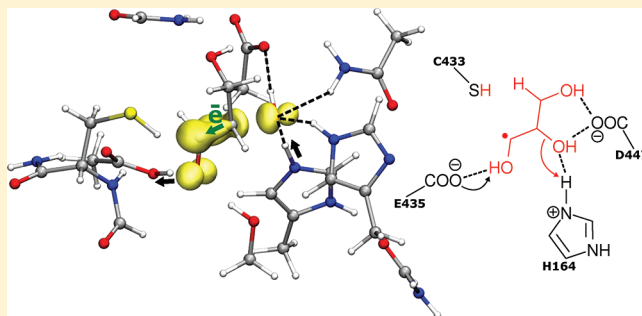
# Glycerol Dehydratation by the $B_{12}$ -Independent Enzyme May Not Involve the Migration of a Hydroxyl Group: A Computational Study

Mikolaj Feliks and G. Matthias Ullmann\*

Computational Biochemistry Group, University of Bayreuth, Universitätsstr. 30, BGI, 95447 Bayreuth, Germany

**S Supporting Information**

**ABSTRACT:** A combination of continuum electrostatic and density functional calculations has been employed to study the mechanism of the  $B_{12}$ -independent glycerol dehydratase, a novel glycyl-radical enzyme involved in the microbial conversion of glycerol to 3-hydroxypropionaldehyde. The calculations indicate that the dehydratation of glycerol by the  $B_{12}$ -independent enzyme does not need to involve a mechanistically complicated migration of the middle hydroxyl group to one of the two terminal positions of a molecule, as previously suggested. Instead, the reaction can proceed in three elementary steps. First, a radical transfer from the catalytically active Cys433 to the ligand generates a substrate-related intermediate. Second, a hydroxyl group splits off at the middle position of the ligand and is protonated by the neighboring His164 to form a water molecule. The other active site residue Glu435 accepts a proton from one of the terminal hydroxyl groups of the ligand and a C=O double bond is created. Third, the reaction is completed by a radical back transfer from the product-related intermediate to Cys433. On the basis of our calculations, the catalytic functions of the active site residues have been suggested. Cys433 is a radical relay site; His164 and Glu435 make up a proton accepting/donating system; Asn156, His281, and Asp447 form a network of hydrogen bonds responsible for the electrostatic stabilization of the transition state. A synergistic participation of these residues in the reaction seems to be crucial for the catalysis.



## INTRODUCTION

Industry shows an increasing interest in reactions that convert glycerol into 3-hydroxypropionaldehyde or 1,3-propanediol, because 1,3-propanediol is an important precursor for the synthesis of novel polyesters.<sup>1–3</sup> Glycerol is obtained as a main byproduct of the transesterification of plant oils and animal fats. Chemical methods used to date to convert glycerol to 1,3-propanediol involve expensive reagents and toxic intermediates.<sup>4</sup> Biochemically, the transformation from glycerol to 3-hydroxypropionaldehyde is done by glycerol dehydratase (GDH). The product is further transformed by a reductase to 1,3-propanediol using NADH as a cosubstrate (see Figure 1). To date, two classes of GDH are known.<sup>5,6</sup> Both catalyze the reaction through a radical mechanism. The first class involves vitamin  $B_{12}$  as a cofactor. These  $B_{12}$ -dependent GDHs are difficult to handle biochemically because they are rapidly inactivated and thus the cofactor vitamin  $B_{12}$ , a high-cost

molecule, needs to be added to the reacting mixture in excessive amounts to overcome this problem.<sup>4</sup> The second class, the  $B_{12}$ -independent GDHs, involve a glycyl radical in their catalysis and belong to the family of glycyl-radical enzymes. The other members of this family identified to date are pyruvate formate lyase, class III ribonucleotide reductase, benzylsuccinate synthase and 4-hydroxyphenylacetate decarboxylase.<sup>5–9</sup>

The first step of the catalysis by the  $B_{12}$ -independent GDH is the release of a hydrogen atom from glycerol by the cysteinyl radical. This step has already been studied computationally before.<sup>10,11</sup> The key aspect of the dehydratation of glycerol is however the abstraction of the hydroxyl group which eventually is transformed into a water molecule. A putative reaction mechanism of the  $B_{12}$ -independent GDH was suggested by analogy to the  $B_{12}$ -dependent GDH.<sup>12</sup> The mechanism of the latter has been extensively studied, both experimentally and computationally.<sup>13,14</sup> The suggested mechanism involves an intramolecular group transfer where the hydroxyl group of the central carbon migrates through a cyclic transition state to one of the terminal carbons of glycerol. The resulting geminal diol intermediate is unstable and breaks up into water and 3-

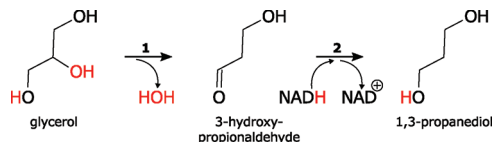


Figure 1. Microbial conversion of glycerol to 1,3-PD: (1) glycerol dehydratase and (2) 1,3-PD dehydrogenase.

Received: February 6, 2012

Revised: May 21, 2012

Published: May 24, 2012

hydroxylpropionaldehyde. However, judging from the crystal structure, this mechanism seems unlikely for the  $B_{12}$ -independent GDH, since the conformation of glycerol found in the active site does not easily facilitate a migration of the hydroxyl group. A migration would require a considerable reorientation of the ligand, which cannot be easily accomplished, because glycerol is locked in the active site by six to seven hydrogen bonds. The active site of GDH contains four titratable residues (Asp447, Glu435, His164, His281) in a direct vicinity of the glycerol ligand. A proper assignment of their protonation states is crucial for understanding the mechanism, because the presence of charged groups in the active site may have a great impact on energy landscape of the reaction. Moreover, such groups may act as proton donors and acceptors during the reaction. The prediction of protonation states of proteins is not an easy task but can be done with reasonable confidence using continuum electrostatics.<sup>15–17</sup>

In this paper, we present a theoretical study on the mechanism of the  $B_{12}$ -independent GDH using continuum electrostatic calculations on the whole protein and quantum chemical calculations on a cluster model.<sup>18–21</sup> On the basis of these calculations, we propose a mechanism of the  $B_{12}$ -independent GDH that does not involve the migration of a hydroxyl group as suggested for the  $B_{12}$ -dependent GDH. We find that the surrounding aminoacids act as proton donors and acceptors, and the reaction can take place without large barriers. The enzyme, which is not accounted for explicitly, is represented by a homogeneous medium with a low dielectric constant, using a conductor-like polarizable continuum model. The proper protonation state of the active site residues was assigned based on electrostatic calculations, a step that is often overlooked in QM or QM/MM studies. However, this step is crucial for the calculations, since the protonation of these residues may determine the reaction mechanism. To keep the notion short we call the  $B_{12}$ -independent GDH just iGDH in the following.

## METHODS

**Calculations of Protonation Probabilities.** The calculations were performed on the glycerol-free form and the glycerol-bound form of iGDH (PDB entry 1r8w and 1r9d,<sup>12</sup> respectively). These structures represent the protein without a radical present in the active site. Crystallization with a radical is not possible, because of the low stability of the radical compared to crystallization time. Each of the two structures consists of a homodimer, in case of the latter with both monomers in a complex with glycerol. For the electrostatic calculations, the structures of the complete dimers were used. Missing hydrogens were added using the HBUILD routine of CHARMM<sup>22</sup> and their positions were subsequently energetically minimized using the CHARMM27 force field,<sup>23</sup> while the rest of the protein was kept fixed. For the minimization of the hydrogens, the protonation states of all titratable residues were set to their standard value at pH 7; histidine residues were assumed to be fully protonated. Also for the subsequent electrostatic calculations, partial charges of the CHARMM27 force field were used. Water molecules were deleted from the system after the optimization. The resulting structures for the glycerol-free and the glycerol-bound form of iGDH were used to calculate the protonation probabilities of all titratable residues. For this purpose, we applied a Poisson–Boltzmann continuum electrostatic model combined with a Monte Carlo titration using MEAD<sup>24</sup> and GMCT.<sup>25</sup> This method has been

successfully used in our lab to study the protonation behavior of a number of different proteins.<sup>26</sup> The following parameters were used in all Poisson–Boltzmann calculations. A dielectric constant of  $\epsilon_p = 4$  was assigned to the interior of the protein; the solvent was modeled as a medium with a dielectric constant of  $\epsilon_s = 80$ , an ionic strength of  $I = 100$  mM and a temperature of  $T = 300$  K. A dielectric constant of  $\epsilon_p = 4$  for the interior of a protein is used in many studies and enables a reliable prediction of the titration behavior of buried and active site residues.<sup>27–34</sup> An ion exclusion layer of 2.0 Å and a solvent probe radius of 1.4 Å were used to define the volume of the protein. The electrostatic potential was calculated using a grid of 121<sup>3</sup> points with four focusing steps at a resolution of 2.0, 1.0, 0.5, and 0.25 Å. The larger grid was geometrically centered on the molecule or complex, while the finer grids were geometrically centered on the group of interest. The protonation probability of all residues was calculated by a Metropolis Monte Carlo algorithm as a function of pH. The pH was varied from 0 to 14 in steps of 0.2 pH-units. For every pH-step, the MC calculation consisted of 100 equilibration scans and 100 000 production scans at  $T = 300$  K.

**Construction of the Cluster Model.** To construct a cluster model of the active site, a molecular mechanics (MM) model was created from the monomer represented by chain A of the glycerol-bound form of iGDH. The protonation states of titratable residues were set according to the previous electrostatic calculations performed for the dimer. The model was prepared using Leap and Antechamber<sup>35</sup> tools from Amber10<sup>36</sup> software package and in-house scripts. The AMBER99 force field<sup>37</sup> was used to describe the protein part. The parameters for glycerol were assigned from GAFF<sup>38</sup> and partial charges were taken from the literature.<sup>39</sup> Cys433 (thiyl radical) was treated as the model residue CYX from the AMBER99 force field. After the addition of missing hydrogens, the complete model consisted of 13817 atoms (786 residues, 493 water molecules, and one glycerol ligand). The system was subsequently subjected to the MM-optimization using Amber10. The optimization was carried out in two steps. In the first step, non-hydrogen atoms were kept frozen and only hydrogens were allowed to move. In the second step, all atoms were set flexible and the system was fully optimized. The final MM-model after optimization did not display any significant differences in geometry with respect to the starting X-ray structure. The rmsd between the structures before and after the optimization was calculated to be 0.51 Å for the whole protein, 0.34 Å for the protein backbone and 0.24 Å for the active site only (a set of residues used to construct the cluster model). Hydrogen atoms were excluded from the calculation of rmsd.

The fully MM-optimized geometry of the monomer was used as a starting point for the DFT study. As a model of the active site, the side chains of eight residues, a short fragment of the protein backbone and the glycerol ligand were selected. Seven residues are located in a direct vicinity of the ligand. These are Asn156, His164, His281, Ser282, Cys433, Glu435, and Asp447. His164 is doubly protonated and His281 is protonated at N<sub>e2</sub>. Glu435 and Asp447 are deprotonated. In addition, a side chain of the second-shell residue Gln549 and a part of the backbone between Val162 and Gly163 were included. These groups were selected for two reasons, first to stabilize the charges on Asp447 and His164 and second to provide additional spatial restraints to the inner parts of the cluster. The final QM-model consisted of 96 atoms and had a total charge of -1.

### Quantum Chemical Calculations on the Cluster Model.

All QM calculations were performed using the B3LYP<sup>40–43</sup> density functional theory method as implemented in Gaussian03<sup>44</sup> software package. The B3LYP functional provides a reasonable balance between accuracy and computational cost which is especially important in studies of cluster models, because their size is often prohibitive for most ab initio methods. This method has also proven to be successful in a number of different studies on radical-containing enzymes.<sup>45</sup> The energies discussed in this paper were calculated using a standard split-valence tripleζ 6-311+G(2d,2p) basis set, unless stated otherwise. For geometry optimizations, a medium-sized 6-31G(d) basis set was used. This basis set is usually sufficient to obtain reliable geometries. The energy of these molecular geometries can then be evaluated by single-point calculations using a larger basis set. This strategy is reliable and significantly reduces the computational expense. The 6-31G(d) basis set was also used in the previous QM/MM study to describe the active site region.<sup>10</sup> The analyses of frequencies and solvation effects were carried out at the same level as geometry optimizations. Zero-point vibrational energy corrections (ZPVE) were estimated from Hessians and added to the energies obtained from the larger basis set. Solvation effects were calculated using a conductor-like polarizable continuum model (CPCM).<sup>46</sup> These effects were included in the final energies in a similar way as ZPVE corrections. Different dielectric constants (2, 4, 8, 16, 80) were used to represent the solvent. Atomic charges and spin densities discussed herein were calculated using the Mulliken population analysis and the larger basis set.

To maintain the integrity of the model, several atoms were kept fixed at their MM-optimized positions during the geometry optimizations. Special care was taken for selecting these atoms. To properly model an enzymatic system, the geometry of the truncated model should be kept close enough to the crystal structure but should also allow a certain extent of flexibility. In our case, eleven out of total ninety-six atoms of the model have been fixed. These are the atoms at positions where the truncation has been made or where it was necessary to compensate for the lack of stabilizing interactions from the rest of the enzyme (see Figure 2). Since the frequency analysis was performed on top of constrained structures, it gives rise to a few imaginary frequencies with no physical meaning. However, for the present cluster model they were all found to be very small and never exceeding  $45i\text{ cm}^{-1}$ . Since their contribution to the ZPVE is marginal, they can be safely ignored.

To test the reliability of the model, a large number of calculations with different sets of constraints was performed. We also studied how the model is affected when additional fragments or residues are added or removed. For example, we analyzed the situation when His281 or Asn156 are not included. Since they do not participate directly in the reaction, that is, they are not involved in any process of bond breaking or forming, one can suppose that none of them is strictly required as a part of the reacting system. However, both residues turned out to be important for the overall stability of the model and could not be easily removed.

The comparison between geometries of the QM-optimized cluster model and the MM-optimized full-enzyme model clearly shows their close resemblance, which further underlines the reliability of the cluster model used. The main structural differences are found for the side chain of Gln549 and for the backbone fragment between Val162 and Gly163. Although their conformations are slightly distorted with respect to the

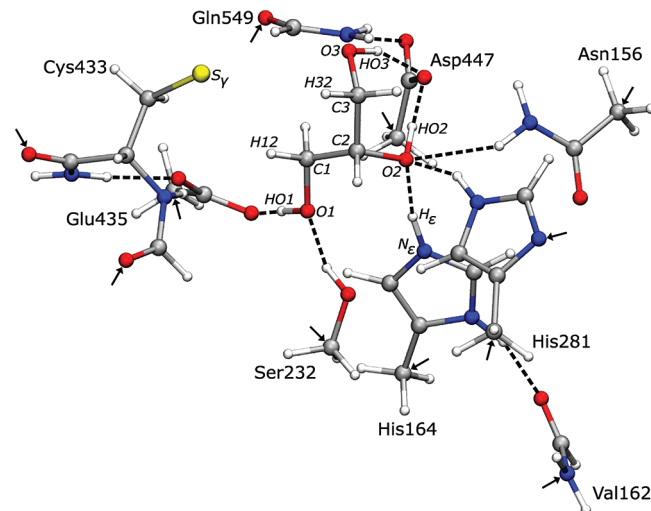


**Figure 2.** QM-optimized model of the active site (reactant state, Sub). Atoms marked with small arrows were kept frozen during the geometry optimizations. Hydrogen bonds are represented by dashed lines. Atoms discussed in the text are labeled.

MM-model, key intermolecular distances are preserved. Also, these fragments are distant enough from the reacting part of the system and the distortions should not have any substantial effect on the mechanism. The conformation of Asn156 varies slightly; the distance between one hydrogen of its amide group and the C2 hydroxyl group of glycerol is shortened by 0.5 Å after the QM optimization. These small differences may well be justified by the flexibility of the enzyme. The overall rmsd of the active site between the MM- and QM-optimized models is 0.47 Å (0.26 Å without second-shell parts, that is, Asn156, Val162, and Gln549). Hydrogen atoms were not included in the calculation of rmsd.

A common problem in the modeling of complex systems, such as large cluster models, is their multidimensionality which leads to a great number of local geometric minima. To ensure that the calculated minima and transition states on the potential energy surface represent the actual reaction path, we studied their nature in detail by frequency analysis, visual inspection and by performing appropriate scans. Special attention was paid to the transition states, which were usually calculated in a following multistep way. First, an energy scan starting from the previously found minimum was performed along the assumed major component of the reaction coordinate, for example a distance between two atoms. Next, two structures from the scan were selected, one of the highest energy and a second from the final point. These structures were used as starting points in the subsequent optimizations to find the transition state and the second minimum. The calculated geometry of a transition state was accepted if only one of its frequencies was negative which is related to the reaction coordinate of interest. In the last step, each transition state was recalculated from the known geometries of two minima using the QST2<sup>47</sup> method followed by an additional frequency analysis.

## RESULTS AND DISCUSSIONS

**Protonation States of Active Site Residues.** The setting of the correct protonation state of the residues in the active site is a crucial step for the modeling of the reaction. Therefore, we performed continuum electrostatic calculation combined with a Monte Carlo sampling. The active site contains several tightly

interacting protonatable residues. In fact, four out of seven residues surrounding the ligand are protonatable (His164, His281, Glu435, Asp447). From our calculations, we found that in the most probable protonation state of the glycerol-bound form of iGDH Glu435 and Asp447 are deprotonated at pH = 7, His281 is single protonated at N<sub>ε2</sub> (uncharged), and His164 is doubly protonated (charged). Interestingly, a proton transfer between the active site residues is possible at relatively low energetic costs. For instance, the transfer of a proton from His164 to Glu435 requires only 0.7 kcal/mol or the transfer of a proton from His164 to Asp447 requires only 2.5 kcal/mol.

An analysis of the crystal structure helps to rationalize the results (see Figure 3). The two negatively charged residues,

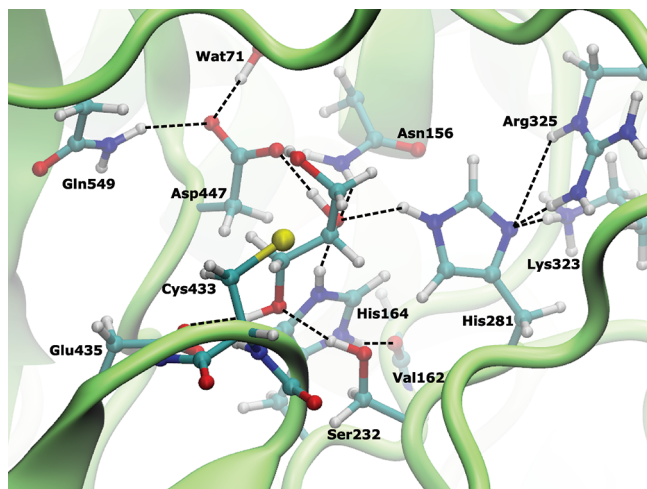


**Figure 3.** Interactions inside the active site of iGDH. His281 is protonated at N<sub>ε2</sub> and hydrogen-bonded at N<sub>ε2</sub> to two positively charged residues, Lys323 and Arg325. His164, which is essential for the reaction, is doubly protonated. It is stabilized by the protein backbone at Val162 on one side and by the negatively charged Asp447 on the other side. His164 and Asp447 can exchange a proton by the intermediacy of the C2 hydroxyl group of glycerol. The negative charge on Asp447 is stabilized also by the interactions with Gln549 and Wat71. The negatively charged Glu435 forms hydrogen-bonds with the C1 hydroxyl group of glycerol and the backbone of Cys433.

Glu435 and Asp447, and the positively charged residue His164 stabilize each other. The positive charge of His164 is further stabilized by a hydrogen bond with the backbone carbonyl oxygen of Val62. The negative charge on Asp447 is stabilized by at least three hydrogen bonds, two from glycerol and one from Gln549, but also the backbone amide of Ala449 and a water molecule may form additional hydrogen bonds. The negative charge of Glu435 is stabilized by two hydrogen bonds from backbone amides, namely of Cys433 and Val434, and a hydrogen bond from glycerol. In contrast, His281, which is according to our calculations uncharged, interacts strongly with two positively charged residues, namely Arg325 and Lys323. This interaction prevents the protonation of His281 even if it is in the vicinity of two negatively charged residues.

**Calculated Reaction Mechanism.** From our analysis, we found that the conversion of glycerol proceeds in three elementary steps in two different though similar reaction paths. The overall reaction mechanism is summarized in Figure 4.

The reaction starts with the ligand bound inside the binding pocket and the catalytically active residue Cys433 is in its neutral radical form. The active site residues form an extensive

network of hydrogen bonds in which the ligand is anchored (see Figure 2 for a structural model and for naming conventions). The hydroxyl group at C1 of glycerol is hydrogen-bound to Glu435 and Ser282. Asp447 binds the second terminal hydroxyl group at C3. Interestingly, the hydroxyl group at C2, that is, the hydroxyl group that will be cleaved off, interacts with four residues, namely with Asp156, His164, His281, and Asp447. These interactions may well be important not only for binding but also for catalysis.

Starting from the substrate, the reaction can proceed along two different paths. In both cases, the radical cysteine abstracts hydrogen at the C1 position of glycerol. The difference between the two paths is the protonation of Asp447 and His164. While in what we call path A, Asp447 is deprotonated and His164 is protonated, the situation is reversed in what we call path B. An initial proton transfer between His164 and Asp447 is easily possible through the hydroxyl group at C2 of the glycerol ligand. According to our electrostatic calculations, the energy difference between these two states is only about 2.5 kcal/mol. Our quantum chemical calculations on the cluster model corroborate this finding. In both protonation states, a hydrogen could also be abstracted at the position C3, but this reaction is associated with a somewhat higher barrier and more importantly leads to an intermediate from which we found no further productive steps (see the section “unproductive steps”).

**Radical Transfer from Cys433 to Glycerol (Step I).** In step I, the catalytically active Cys433 abstracts hydrogen from the ligand and a substrate-derived radical intermediate is formed (Sub → TS1 → In1 in Figure 5). The initial distance between the S<sub>γ</sub> of Cys433 and the hydrogen at C1 of glycerol is shortened from 2.99 to 1.53 Å in the transition state. The resulting geometry of the intermediate is similar to that of the substrate. For reaching the substrate, only the distance between C2 and O1 decrease from 1.42 to 1.36 Å. All other geometrical changes are small. The calculated activation energy for the initial radical transfer is 10.3 kcal/mol and the reaction energy is +4.8 kcal/mol (see Table 1).

Since the enzymatic environment can lower the activation energy, we performed a series of calculations using the conductor-like polarizable continuum method in which a homogeneous medium is used to represent the presence of the protein environment (see Tab. 1). The barrier slowly reduces with an increasing value of the dielectric constant, i.e. with increasing polarity of the environment. For  $\epsilon = 4$ , which is typically used for modeling protein interiors, the barrier is lowered by only 1.9 kcal/mol. Interestingly, the reaction energy remains stable and even at the dielectric constant of 80 its value is only 0.4 kcal/mol lower than in vacuum. A possible explanation is that the geometry and more importantly, charge distribution of the substrate and the first intermediate are nearly the same (see Tab S1 in Supporting Information). Therefore, they respond in the same way when exposed to environments of different polarizability. Consequently, the solvation energy of the first intermediate and of the substrate will be similar, no matter what the dielectric constant of the solvent is. As suggested by Himo and co-workers,<sup>48</sup> the stability of barriers and reaction energies over a wide range of values for the dielectric constant may indicate that the cluster is chosen large enough, because the solvation effects have already saturated at its present size and no catalytically important parts are missing from the model.

From the analysis of calculated spin density, it can be seen that the reaction starts with the radical localized exclusively at

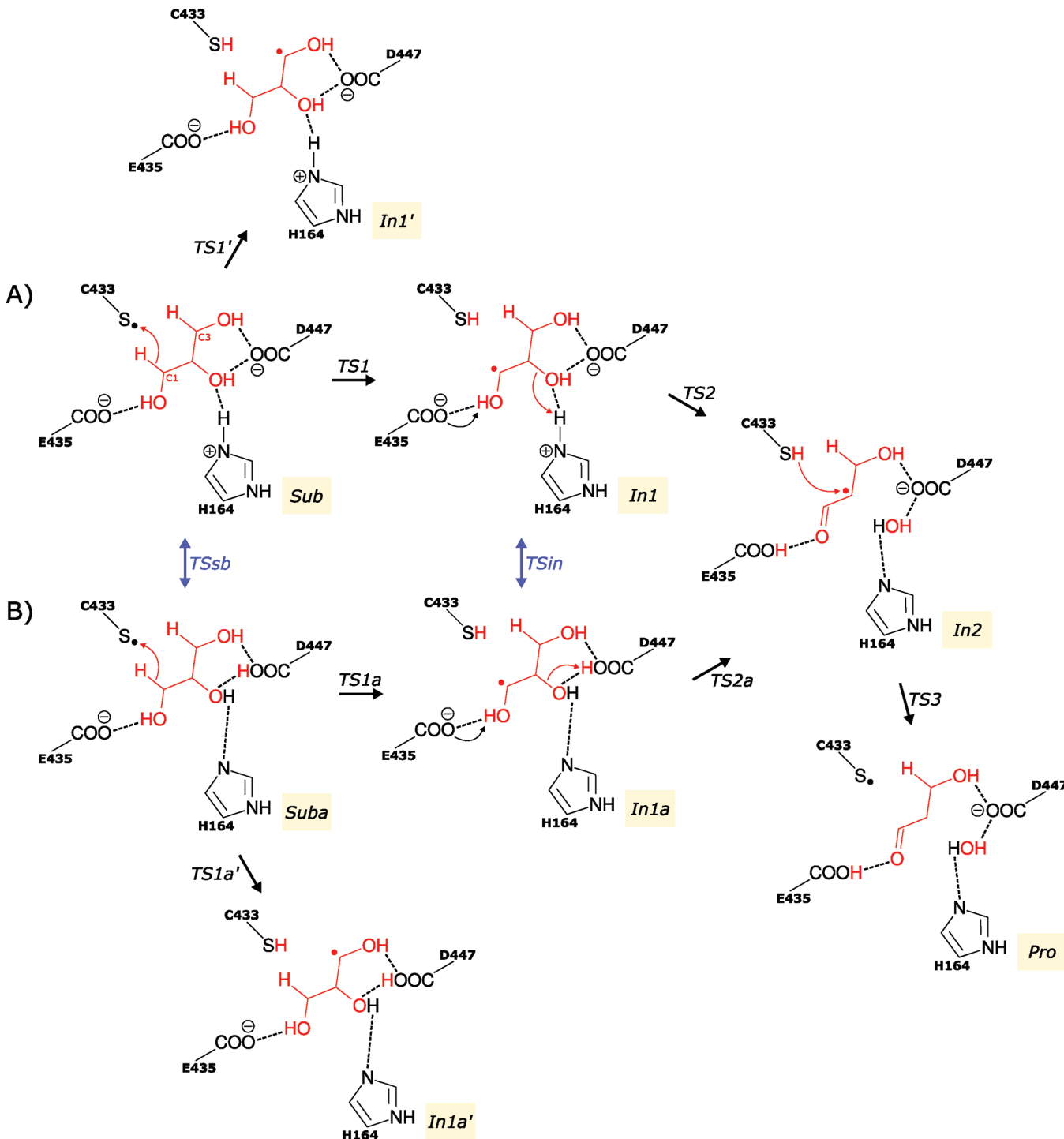


**Figure 4.** Mechanism of iGDH as derived from the calculations. Blue arrows indicate possible interconnections between both paths. For clarity, only the arrows corresponding to the movement of electrons of the main reaction were shown. In the alternative path B the proton transfer His164 → ligand → Asp447 (TSsb) precedes the radical transfer. Path B can also be accessed from the substrate-derived intermediate of path A (TSin). From Sub and Suba, the reaction can also proceed through TS1' and TS1a', respectively. However, it cannot proceed from that point any further.

the sulfur atom of Cys433. This observation is consistent with many other computational studies on cysteine-radical containing enzymes.<sup>49</sup> After the abstraction of a hydrogen atom by Cys433, the radical is localized at the ligand and is shared mainly between C1 and O1 atoms. The corresponding atomic spin densities are 0.87 and 0.12, respectively (In1 on Figure 5).

**Dehydratation of the First Intermediate (Step II).** The bond between the atoms C2 and O2 of the electron-deficient

intermediate In1 becomes weak and the reaction can proceed to the second stage (In1 → TS2 → In2 in Figure 5). Unlike for the hydrogen abstraction in step I, dehydratation is mechanistically more complicated and involves a simultaneous movement of two protons, breaking of the bond between C2 and O2, formation of the double bond between C1 and O1 and formation of a water molecule. The major structural change in step II is an elongation of the bond between C2 and O2 from

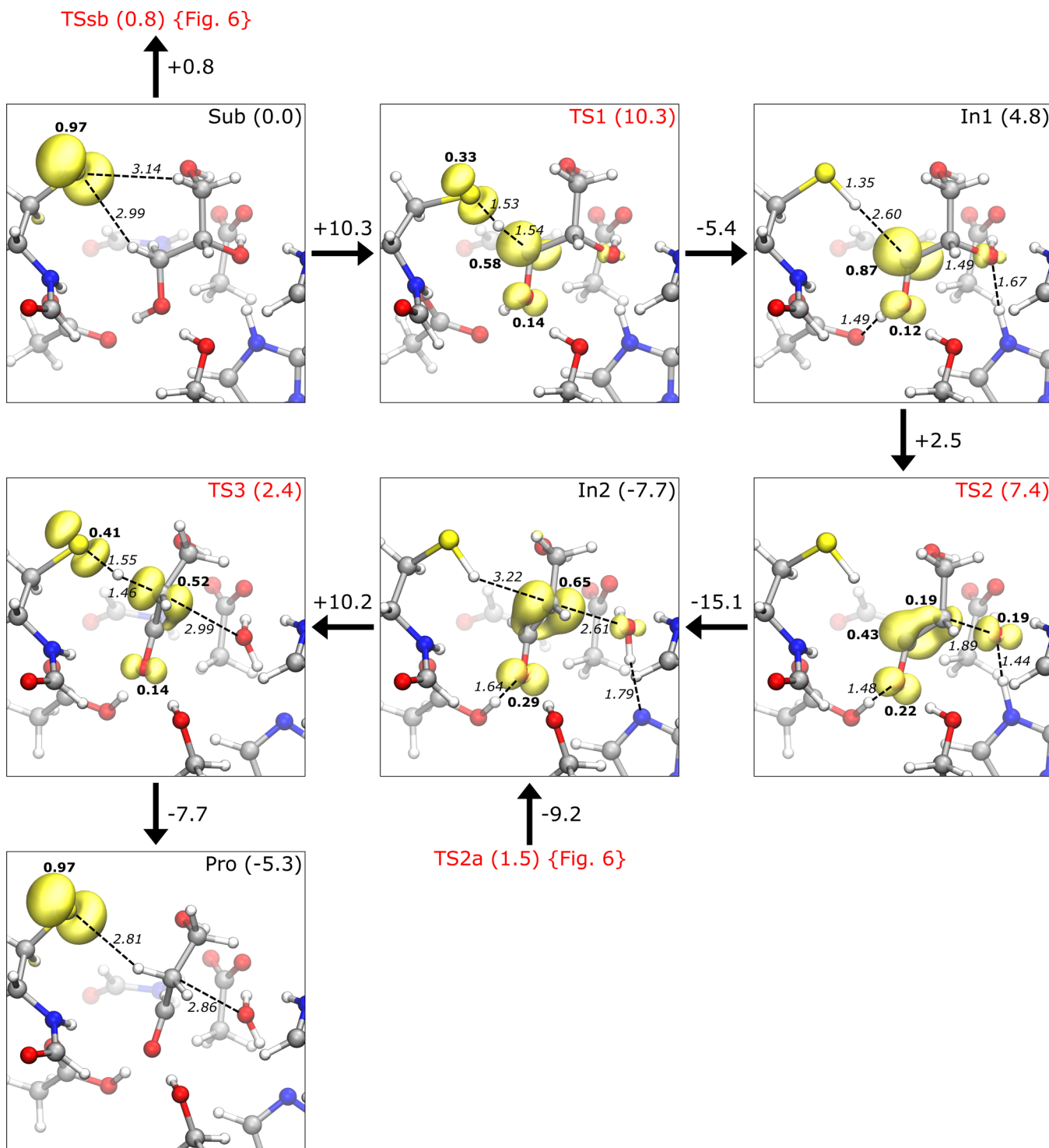


**Figure 5.** Optimized geometries of intermediates and transition states for path A. For clarity, only the most important part of the reacting system was shown. Intra- and intermolecular distances relevant for each reaction step are given in angstrom ( $\text{\AA}$ ). Small bold numbers are the Mulliken atomic spin densities. For the 3D spin density the isovalue of 0.01 au was used. All structures are given with the energies (kcal/mol) relative to the reactant state (sub). Transition states are marked with red labels. Values at the arrows indicate changes of the energy.

1.49 to 1.89  $\text{\AA}$  in the transition state (TS2). The bond is further extended to 2.61  $\text{\AA}$  in the second intermediate (In2). This step is also linked to a significant charge redistribution, because two charged groups become neutral; these are His164 and Glu435. The proton originally bound to His164 forms together with O2 and HO2 of the ligand a water molecule. Glu435 receives a proton from O1, which leads to the formation of a keto group.

Interestingly, the optimized geometry of the second transition state TS2 shows the HO1 proton already bound to Glu435. It may indicate that the proton transfer between the hydroxyl group of the ligand and Glu435 is a factor triggering the dehydratation.

The barrier associated with step II was calculated to be only 2.5 kcal/mol. From Table 1, it can be seen that this barrier is

**Table 1. Summary of the Reaction Energetics (kcal/mol) Calculated in Vacuum and in a Series of Environments of Increasing Polarity<sup>a</sup>**

		vacuum	$\epsilon = 2$	$\epsilon = 4$	$\epsilon = 8$	$\epsilon = 16$	$\epsilon = 80$
path A							
Sub → In1	$\Delta E^\ddagger$	10.3	9.1	8.4	8.0	7.8	7.7
	$\Delta E$	4.8	4.5	4.5	4.4	4.4	4.4
In1 → In2	$\Delta E^\ddagger$	2.5	4.4	5.3	5.7	5.9	6.1
	$\Delta E$	-12.6	-9.9	-8.6	-8.0	-7.7	-7.4
In2 → Pro	$\Delta E^\ddagger$	10.2	10.1	9.8	9.7	9.6	9.5
	$\Delta E$	2.4	2.7	2.7	2.8	2.8	2.8
path B							
Suba → In1a	$\Delta E^\ddagger$	9.6	8.6	7.9	7.6	7.4	7.2
	$\Delta E$	3.2	2.9	2.9	2.9	2.9	2.9
In1a → In2	$\Delta E^\ddagger$	0.4	2.0	2.6	2.9	3.1	3.2
	$\Delta E$	-8.8	-10.0	-10.7	-11.1	-11.3	-11.5
interconnections							
Sub → Suba	$\Delta E^\ddagger$	0.8	3.4	4.7	5.4	5.8	6.0
	$\Delta E$	-2.1	1.7	3.7	4.7	5.2	5.5
In1 → In1a	$\Delta E^\ddagger$	0.4	2.9	4.3	5.1	5.4	5.7
	$\Delta E$	-3.8	0.1	2.1	3.1	3.7	4.1
unproductive steps							
Sub → In1'	$\Delta E^\ddagger$	14.6	14.5	14.7	14.7	14.8	14.8
	$\Delta E$	5.2	6.0	6.7	7.0	7.2	7.4
Suba → In1a'	$\Delta E^\ddagger$	10.7	16.0	19.0	20.6	21.4	22.0
	$\Delta E$	0.0	5.9	9.3	11.1	12.0	12.8

<sup>a</sup> $\Delta E^\ddagger$  and  $\Delta E$  are the activation energy and reaction energy, respectively. All values were calculated at the B3LYP/6-311+G(2d,2p) level on top of the geometries optimized at the B3LYP/6-31G(d) level. Zero-point corrections and solvation effects were evaluated at the same level as geometry optimizations. Note: In case of Sub → In1' and Suba → In1a', Asn156 was removed from the model (for the reasons explained in the text).

also relatively sensitive to the changes of the dielectric constant. It raises from 2.5 to 5.3 kcal/mol considering a dielectric constant of 4 which resembles the protein interior and even further to 6.1 kcal/mol for a highly polar medium like water.

As we discussed above, the network of hydrogen bonds provides electrostatic interactions which hold the ligand inside the active site. In particular, the leaving hydroxyl group is hydrogen-bound with His164, His281, Asn156, and Asp447. Also Ser344 is a residue which may have some catalytic contribution to step II, because it forms a hydrogen bond to the C1 hydroxyl group of the ligand. To further investigate the effect of these hydrogen bonds, we performed single-point energy calculations for the truncated models of In1 and TS2 where either Asn156, His281, or Ser344 have been removed. We used the geometries of the complete models and deleted the respective atoms, that is, no additional optimizations were done. The calculations were performed at the B3LYP/6-311+G(2d,2p) level. We found that the activation energy raises after the removal of Asn156 and His281 by 1.6 and 2.5 kcal/mol, respectively. When both residues are removed, the barrier increases by 4.6 kcal/mol. The removal of Ser344 gives the barrier elevated by 1.2 kcal/mol, which is only a minor catalytic effect. Thus, Ser344 is probably more important for binding and orienting glycerol inside the active site. This residue may be responsible for holding the C1 hydroxyl group in a position suitable for the proton transfer to Glu435.

The single-point calculations on the truncated models confirm that hydrogen bonding plays an important role in step II. Clearly, the electrostatic stabilization of the transition state is a considerable effect which can lower the barrier by several kcal/mol.

**Transfer of the Radical Back to Cys433 (Step III).** To complete the reaction, the second intermediate In2 needs to

abstract a hydrogen atom from Cys433 (In2 → TS3 → Pro on Figure 5). When this abstraction is accomplished, the resulting final product 3-hydroxypropionaldehyde can be released from the active site. In the second intermediate, the radical is localized mainly at the position C2 of the ligand, to where the hydrogen atom should be delivered (atomic spin density 0.65). A slightly longer distance than before has to be overcome to accomplish the hydrogen atom transfer (3.21 Å). However, the activation energy was calculated to be 10.2 kcal/mol, which is very similar to that of step I. Thus, step I and step III can be both rate determining. Unlike for the first two steps, the barrier of the final transfer is now almost completely unaffected by the changes of the dielectric constant and is at  $\epsilon = 80$  only 0.7 kcal/mol lower than in a nonpolar environment ( $\epsilon = 1$ ). This finding further confirms the completeness of the model but can also show that the electrostatic effects are of minor importance in the last reaction step.

An important observation is that now the ligand is held in the active site by only two hydrogen bonds. Thus, less energy is required to bring the ligand closer to Cys433 in the transition state, because the hydrogen bond network does not have to be stretched as much as before. Because of the lack of the hydrogen bonds, the product can also leave the active site more easily after the final radical transfer is complete.

The proposed mechanism of dehydratation requires the regeneration of the active site to its initial state, because the protonation of Glu435 and His164 at the end of the reaction is different from that at the beginning. In the crystal structure of glycerol-free iGDH, two water molecules replace the ligand and form a bridge of hydrogen bonds connecting Glu435 and His164. This bridge can facilitate a proton transfer between these residues and help to recreate the catalytically active state before binding a new ligand. Alternatively, the proton can move

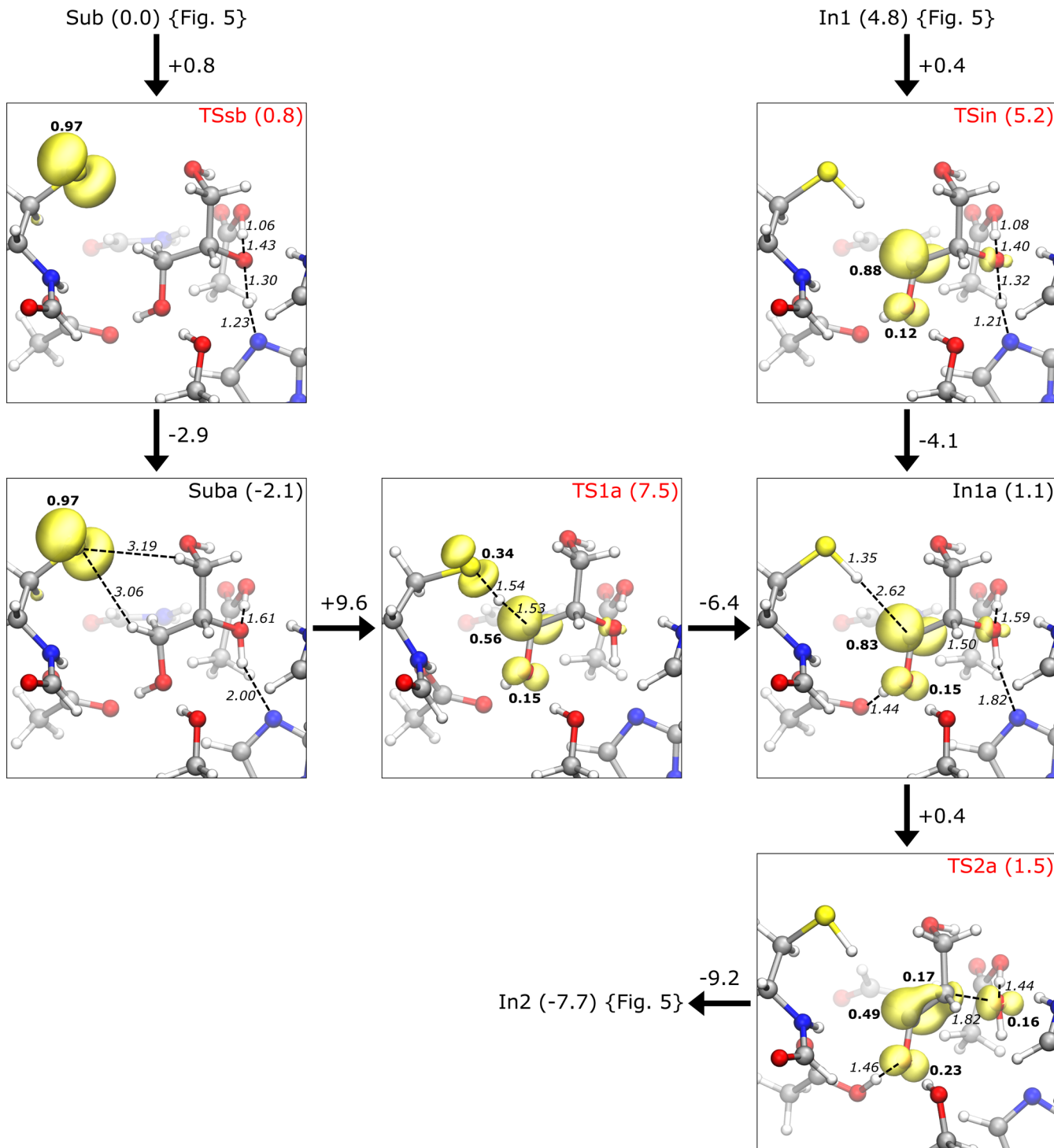


**Figure 6.** Alternative path (B) can be accessed by a proton transfer His164 → ligand → Asp447 either from Sub or In1 of path A. Both entries eventually lead to the intermediate In1a and transition state TS2a. Once TS2a is passed, the reaction proceeds as in path A.

from Glu435 to His164 when glycerol is bound. In this case, the OH group bound to C1 of glycerol would function as bridge.

**Alternative Reaction Path.** In our exploration of possible reaction mechanisms, we found an alternative although similar path. In this path, first a proton transfer from His164 to Asp447 occurs. As a result, these two residues become neutral and in the subsequent dehydration Asp447 acts as a proton donor instead of His164. The energetics of this path, which we call

path B, is shown in Table 1. The previously discussed path is called path A.

The proton transfer from His164 to Asp447 is mediated by the C2 hydroxyl group of glycerol (**Sub → TSsb → Suba** in Figure 6). To reach the transition state, two protons have to move simultaneously. These are the proton bound to N<sub>e2</sub> of His164 and the proton bound to O2 of glycerol. The reaction energy for this proton transfer in a dielectric medium with  $\epsilon = 2$  is 1.7 kcal/mol and with  $\epsilon = 4$  is 3.7 kcal/mol. These values are in good agreement with a value of 2.5 kcal/mol which we

obtained from electrostatic calculations on the whole protein. In vacuum, the transfer is almost barrierless (0.8 kcal/mol), but in a low dielectric environment ( $\epsilon = 4$ ) the barrier raises to 4.7 kcal/mol and further to 6 kcal/mol at  $\epsilon = 80$ . By analogy to step II of path A, a higher barrier can be explained by the weakening of the electrostatic interactions that stabilize the transition state. Path B can be accessed in a similar way from In1 (In1 → TSin → In1a on Figure 6). The dehydratation on path B is associated with a barrier that is about 2 kcal/mol lower than in path A (In1a → TS2a → In2 in Figure 6). The release of water results in a formation of the same intermediate In2 as in path A; that is, when the second intermediate is reached, both paths merge. In a dielectric medium, path B is energetically higher than path A. The barriers in path A and B are similar, especially for the first step which has a relatively high barrier. Thus in a protein, the reaction path A seems more likely.

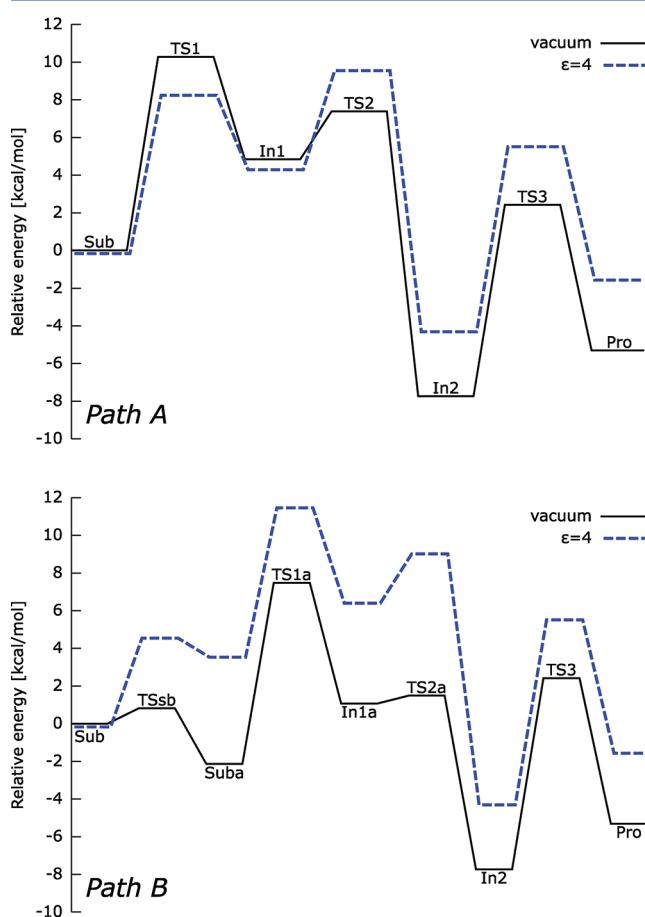


**Figure 7.** Reaction profiles of path A (above) and path B (below) in vacuum and in a protein environment.

**Unproductive Steps.** In principle, the reaction can also start with the abstraction of a hydrogen atom bound at the position C3 of glycerol. In the optimized geometry of the substrate, the distance between the atoms  $S_{\gamma}$  of Cys433 and H31 of glycerol is 3.14 Å, which is only slightly longer than between  $S_{\gamma}$  and H12 which is 2.99 Å. However, 1,2-propanediol is also a good substrate of iGDH. It has been shown crystallographically that 1,2-propanediol binds with its hydroxyl group at C1 near Glu435.<sup>12</sup> This finding makes it unlikely that the hydrogen atom is abstracted from C3 of glycerol.

To check whether the abstraction of the H31 hydrogen atom of glycerol would be possible, a new cluster model had to be constructed. The cluster model used so far was found inappropriate for this case, because the optimization to the transition state TS1' resulted in a movement of Asn156 toward the carboxyl group of Asp447 that would be sterically impossible in the enzyme. To prevent the unwanted behavior of Asn156, one can apply more constraints to the model by fixing additional atoms. Instead, we decided to remove this residue completely. We validated the use of the new cluster model by analyzing the influence of Asn156 on the hydrogen atom abstraction from C1 of glycerol. The energy differences was always less than 1 kcal/mol. From our calculations, we find barriers in vacuum for the abstraction from C3 that are 4.5 kcal/mol higher than for the abstraction from C1 (see Table 1). While the barrier for the hydrogen abstraction from C1 could be lowered after the inclusion of solvent effects, this was not the case for the hydrogen abstraction from C3. The higher barrier seems to originate from geometrical reasons. In the substrate state, the distances from  $S_{\gamma}$  of Cys433 to H12 (2.99 Å) and H32 (3.14 Å) of glycerol are similar (see Figure 5). However, H12 is in a better position for the abstraction, because the angle  $C_{\beta}-S_{\gamma}-H12$  (which is 85°) is closer to the equilibrium value of a standard C–S–H angle (which is about 95°) than the angle  $C_{\beta}-S_{\gamma}-H32$  which is 134°. In the transition state TS1 (or TS1a), the transfer of a hydrogen atom occurs at a more favorable angle of 99°. In TS1' (or TS1a') the transfer occurs at an angle of 107°, which leads to an elevated barrier.

Starting from the intermediate In1' or In1a', a relaxed energy surface scan along the C2–O2 bond was performed in order to estimate the geometry of an expected transition state. The bond was extended in steps of 0.1 Å. Unlike for the mechanism described before, the scan resulted in an ever-increasing energy and no transition state could be localized. In the case of a hydrogen atom abstraction from C3, Asp447 is expected to replace Glu435 as a proton acceptor. However, the orientation of Glu435 toward the C1 hydroxyl group is far more favorable than the orientation of Asp447 toward the C3 hydroxyl group. In particular, the transfer of the HO1 proton can be accomplished easily, because this atom is positioned on the same plane as the carboxylic group of Glu435. On the other hand, the HO3 hydrogen is nearly 60° out of the plane which is formed by the carboxylic group of Asp447. Our finding that the hydrogen atom abstraction from C1 is preferred corroborates previous results from the QM/MM study by Liu and co-workers.<sup>10,11</sup> Thus, the reaction can proceed only from In1 (or In1a), because the active site favors by its geometry a proton transfer between C1 hydroxyl group and Glu435.

**Comparison of iGDH to Related Enzymes.** Interestingly, the calculated mechanism of the  $B_{12}$ -independent GDH is similar to the mechanism of another glycyl-radical enzyme, namely, the anaerobic ribonucleotide reductase (class III RNR or simply ARNR).<sup>50</sup> Both, iGDH and ARNR, catalyze the reaction that at some point involves the release of a hydroxyl group from the ligand and formation of a water molecule.

In the case of ARNR, a ribonucleotide ligand is activated by the abstraction of the 3'-hydrogen atom by the radical cysteine. In the next step, the hydroxyl group at the position 2' splits off from the ligand and is protonated by the formate cofactor. The cofactor subsequently accepts a proton from the second hydroxyl group and a 3'-carbonyl group is formed. The release of water shifts the radical from the position 3' to 2'. Another

catalytically active cysteine delivers a hydrogen atom to the position 2' and deactivates the ligand.<sup>51,52</sup>

In the case of iGDH, we propose that glycerol is activated by the abstraction of the H12-hydrogen atom by Cys433. The hydroxyl group at the position C2 is released from the ligand and gets protonated by His164. Glu435 accepts a proton from the hydroxyl group at the position C1 which leads to formation of a carbonyl group. The loss of water shifts the radical from the position C1 to C2. This step is followed by transfer of the hydrogen atom from Cys433 back to the ligand, which completes the reaction.

In ARNR, formate functions as a cofactor which first delivers a proton to the 2'-hydroxyl group and then accepts a proton from the 3'-hydroxyl group. This cofactor is analogous to the pair of residues His164 and Glu435 that are found in the active site of iGDH. The positively charged His164 delivers a proton to the leaving hydroxyl group (Asp447 can replace His164 on the reaction path B). Glu435, on the other hand, is a proton acceptor responsible for the formation of the carbonyl group at the C1 position of glycerol. The difference between iGDH and ARNR is that the former uses two active site residues as a proton donating-accepting system and the latter uses only formate.

$B_{12}$ -independent GDH and  $B_{12}$ -dependent GDH belong to different enzyme families, but both adopt a radical-mediated mechanism for the dehydration of glycerol. The  $B_{12}$ -dependent GDH employs an adenosylcobalamin cofactor directly in the catalysis; the  $B_{12}$ -independent GDH is a glycyl-radical enzyme that activates the substrate by intermediacy of the radical cysteine. In this work, we propose that the mechanism of iGDH may be different to the one that is suggested for the  $B_{12}$ -dependent GDH. Namely, the mechanism of iGDH may not involve an intramolecular migration of the hydroxyl group within the ligand. On the other hand, the active sites of both enzymes show many similarities and thus their comparison may lead to deeper insights. We include also the  $B_{12}$ -dependent diol dehydratase (DDH) in this comparison. This enzyme is isofunctional to the  $B_{12}$ -dependent GDH, but has been studied more extensively.<sup>14,53–55</sup>

In our proposed mechanism of iGDH, Glu435 plays a key role because it accepts a proton from the terminal hydroxyl group during the dehydration step. An equivalent residue is present in DDH, namely Glu170, which is also crucial for the catalysis. It temporarily accepts a proton during the step of the –OH group migration. The mutation of Glu170 into alanine results in an enzyme that is totally inactive.<sup>56</sup>

The proposed function of His164 in iGDH is to deliver a proton to the leaving hydroxyl group. Both His164 and Glu435 make up a proton donating-accepting system that is essential for the catalysis by iGDH. His164 is analogous to His143 in DDH.<sup>57</sup> The latter provides partial protonation of the migrating hydroxyl group, the effect that can lower the activation energy of migration by a few kcal/mol. His164 in iGDH is doubly protonated due to the stabilizing interactions from the protein backbone and from the negatively charged Asp447. Unlike the histidine in iGDH, His143 in DDH is believed to be protonated only at N<sub>e2</sub>,<sup>54,55</sup> because important stabilizing interactions from the backbone are missing. Complete donation of a proton to the hydroxyl group of the ligand would result in doubly deprotonated His143 in DDH, which is normally highly unfavorable. Since His164 in iGDH can be easily deprotonated and His143 in DDH cannot, this could be one of the reasons why these enzymes may adopt different mechanisms of

dehydration. The mutation of His143 into alanine has been shown to reduce significantly the activity of DDH.<sup>56</sup> It is not known whether the mutation of His164 to some other residue would have any effect on the activity of iGDH. Since there is a “backup” reaction path available (path B), one can speculate that the activity is sustained after Asp447 takes over the function of missing His164.

Asp335 in DDH is a counterpart of Asp447 in iGDH. The function of Asp335 has not been studied computationally in detail. From mutation experiments, it is known that this residue is also crucial for the catalysis by DDH.<sup>56</sup> Assuming that the mechanism involving migration is the only one that is valid, the role of Asp335 in DDH is most likely related to proper binding of the ligand inside the pocket. Asp447 in iGDH, apart from binding the ligand, can also actively participate in catalysis by replacing His164 on the reaction path B.

There is no second histidine in the active site of DDH. Instead, a potassium ion is located at the position similar to that of His281 in iGDH. This ion is mainly responsible for holding the ligand in the position that is suitable for the reaction. The active site of iGDH shows that there is a tight network of hydrogen bonds from the surrounding residues that hold the ligand in a fixed position. In particular, the leaving hydroxyl group forms four hydrogen bonds. A migration of the hydroxyl group as seen for DDH would require a breaking of all these hydrogen bonds. We have investigated the possibility of the –OH group migration by additional PES scans by shortening the distance between O2 and C1 (or C3) atoms of the substrate-related intermediate (In1 or In1'). However, the energy of these scans is rising to the values far exceeding 20 kcal/mol after the hydrogen-bond network has been stretched only slightly. In the case of DDH, the migrating hydroxyl group is coordinated to His143, to the potassium ion and probably to Asp335. Only the hydrogen bond to Asp335 needs to be stretched during the migration of the hydroxyl group. Unlike His164 in iGDH, His143 in DDH is not coordinated to the backbone and has more flexibility in the active site. Also the interaction from the potassium ion is perpendicular to the line between atoms C2 and C1 along which the migration presumably takes place. The interaction between the hydroxyl group and the potassium ion can be therefore maintained throughout the reaction.

Although intramolecular migration of the hydroxyl group is very plausible for DDH in the few of the experimental results, iGDH may work through a different mechanism. The active site of DDH allows more flexibility to the ligand, but it does not provide a proton donating-accepting system. In case of iGDH, the ligand is tightly locked inside the active site. However, a direct release of the hydroxyl group is possible, because both His164 and Glu435 are directly involved in the catalysis. Thus, the mechanism of iGDH is probably more similar to that of ARNR, which seems not to involve a cyclic intermediate.

## CONCLUSIONS

In this work, we have described the possible mechanism of the  $B_{12}$ -independent GDH different to that proposed earlier by analogy to the  $B_{12}$ -dependent GDH. Most importantly, the mechanism does not require a migration of the middle hydroxyl group to one of the terminal positions of glycerol, as previously suggested. Instead, a direct participation of two protein residues, namely His164 and Glu435, turns out to be crucial for the catalysis. The function of the positively charged His164 is to deliver a proton to the leaving hydroxyl group. Glu435, on

the other hand, is a proton acceptor responsible for the formation of the carbonyl group at the C1 position of glycerol. The rate-limiting steps of the reaction are the initial and the final radical transfer. The activation energy for the dehydratation was found to be within a surprisingly low range of 2–6 kcal/mol (depending on the model used). We performed calculations with increasing values of the dielectric constant and with different model systems. We found that the barrier of the dehydratation is reduced by electrostatic interactions from the neighboring residues. These residues are Asn156, His281, and Asp447. However, electrostatic effects are less important for the first and the last reaction step, since the corresponding barriers remained nearly unaffected by varying the dielectric constant. In summary, the catalytic proficiency of iGDH seems to originate from three different effects, first a radical-assisted catalysis, second the appropriate proton donation/acceptance properties of active site residues, and third the electrostatic stabilization of the transition state.

To test the proposed mechanism, isotope labeling experiment could be performed in which the oxygen atom of the middle hydroxyl group of glycerol is labeled with  $^{18}\text{O}$ . If the calculated mechanism is valid, the  $^{18}\text{O}$ -labeled oxygen should always be released as a water molecule after the reaction is complete. Thus, the occurrence of the  $^{18}\text{O}$ -label in the product, which is seen for the  $\text{B}_{12}$ -dependent enzymes,<sup>58</sup> would disprove our proposed mechanism.

## ASSOCIATED CONTENT

### Supporting Information

Cartesian coordinates for the optimized structures and an MPEG animation showing the reaction path A (linearly interpolated between calculated geometries). This material is available free of charge via the Internet at <http://pubs.acs.org>.

## AUTHOR INFORMATION

### Corresponding Author

\*E-mail: Matthias.Ullmann@uni-bayreuth.de.

### Notes

The authors declare no competing financial interest.

## ACKNOWLEDGMENTS

This work was supported by the DFG grant UL 174/8-2 and the BioMedTec International Graduate School of the Elitenetwork Bavaria.

## REFERENCES

- (1) Deckwer, W. *FEMS Microbiol. Rev.* **1995**, *16*, 143–149.
- (2) Gonzalez-Pajuelo, M.; Meynil-Salles, I.; Mendes, F.; Soucaille, P.; Vasconcelos, I. *Appl. Environ. Microbiol.* **2006**, *72*, 96–101.
- (3) Yazdani, S. S.; Gonzalez, R. *Curr. Opin. Biotechnol.* **2007**, *18*, 213–219.
- (4) Raynaud, C.; Sarcabal, P.; Meynil-Salles, I.; Croux, C.; Soucaille, P. *Proc. Natl. Acad. Sci. U.S.A.* **2003**, *100*, 5010–5015.
- (5) Buckel, W.; Golding, B. T. *Annu. Rev. Microbiol.* **2006**, *60*, 27–49.
- (6) Buckel, W. *Angew. Chem., Int. Ed.* **2009**, *48*, 6779–6787.
- (7) Eklund, H.; Fontecave, M. *Struct. Fold. Des.* **1999**, *7*, R257–R262.
- (8) Selmer, T.; Pierik, A.; Heider, J. *Biol. Chem.* **2005**, *386*, 981–988.
- (9) Martins, B. M.; Blaser, M.; Feliks, M.; Ullmann, G. M.; Buckel, W.; Selmer, T. *J. Am. Chem. Soc.* **2011**, *133* (37), 14666–14674.
- (10) Liu, Y.; Gallo, A. A.; Florian, J.; Liu, Y.-S.; Mora, S.; Xu, W. *J. Phys. Chem. B* **2010**, *114*, 5497–5502.
- (11) Liu, Y.; Gallo, A. A.; Xu, W.; Bajpai, R.; Florian, J. *J. Phys. Chem. A* **2011**, *115*, 11162–11166.
- (12) O'Brien, J.; Raynaud, C.; Croux, C.; Girbal, L.; Soucaille, P.; Lanzilotta, W. *Biochemistry* **2004**, *43*, 4635–4645.
- (13) Toraya, T. *Chem. Rev.* **2003**, *103*, 2095–2127.
- (14) Sandala, G. M.; Smith, D. M.; Radow, L. *Acc. Chem. Res.* **2010**, *43*, 642–651.
- (15) Bashford, D.; Karplus, M. *J. Phys. Chem.* **1991**, *95*, 9556–9561.
- (16) Ullmann, G. M.; Knapp, E. W. *Eur. Biophys. J.* **1999**, *28*, 533–551.
- (17) Bombarda, E.; Ullmann, G. M. *J. Phys. Chem. B* **2010**, *114*, 1994–2003.
- (18) Himo, F. *Theor. Chem. Acc.* **2006**, *116*, 232–240.
- (19) Chen, S.-L.; Fang, W.-H.; Himo, F. *Theor. Chem. Acc.* **2008**, *120*, 515–522.
- (20) Siegbahn, P. E. M.; Himo, F. *J. Biol. Inorg. Chem.* **2009**, *14*, 643–651.
- (21) Siegbahn, P. E. M.; Himo, F. *Wiley Interdiscip. Rev.: Comput. Mol. Sci.* **2011**, *1*, 323–336.
- (22) Brooks, B. R.; Brucoleri, R. E.; Olafson, B. D.; States, D. J.; Swaminathan, S.; Karplus, M. *J. Comput. Chem.* **1983**, *4*, 187–217.
- (23) MacKerell, A.; Bashford, D.; Bellott, M.; Dunbrack, R.; Evanseck, J.; Field, M.; Fischer, S.; Gao, J.; Guo, H.; Ha, S.; et al. *J. Phys. Chem. B* **1998**, *102*, 3586–3616.
- (24) Bashford, D.; Gerwert, K. *J. Mol. Biol.* **1992**, *224*, 473–486.
- (25) Ullmann, R. T.; Ullmann, G. M. *J. Comput. Chem.* **2012**, *33*, 887–900.
- (26) Ullmann, G. M.; Kloppmann, E.; Essigke, T.; Krammer, E.-M.; Klingen, A. R.; Becker, T.; Bombarda, E. *Photosynth. Res.* **2008**, *97*, 33–53.
- (27) Taly, A.; Sebban, P.; Smith, J. C.; Ullmann, G. M. *Biophys. J.* **2003**, *84*, 2090–2098.
- (28) Calimet, N.; Ullmann, G. M. *J. Mol. Biol.* **2004**, *339*, 571–589.
- (29) Becker, T.; Ullmann, R. T.; Ullmann, G. M. *J. Phys. Chem. B* **2007**, *111*, 2957–2968.
- (30) Bombarda, E.; Becker, T.; Ullmann, G. M. *J. Am. Chem. Soc.* **2006**, *128*, 12129–12139.
- (31) Bombarda, E.; Ullmann, G. M. *Faraday Disc.* **2011**, *148*, 173–193.
- (32) Kim, J.; Mao, J.; Gunner, M. R. *J. Mol. Biol.* **2005**, *348*, 1283–1298.
- (33) Song, Y. F.; Gunner, M. R. *J. Mol. Biol.* **2009**, *387*, 840–856.
- (34) Zhang, J.; Gunner, M. R. *Biochemistry* **2010**, *49*, 8043–8052.
- (35) Wang, J.; Wang, W.; Kollman, P. A.; Case, D. A. *J. Mol. Graph. Model.* **2006**, *25*, 247–260.
- (36) Case, D. A.; Darden, T. A.; Cheatham III, T. E.; Simmerling, C. L.; Wang, J.; Duke, R. E.; Luo, R.; Crowley, M.; Walker, R. C.; Zhang, W.; et al. *Amber 10*; 2008.
- (37) Hornak, V.; Abel, R.; Okur, A.; Strockbine, B.; Roitberg, A.; Simmerling, C. *Proteins* **2006**, *65*, 712–725.
- (38) Wang, J.; Wolf, R.; Caldwell, J.; Kollman, P.; Case, D. *J. Comput. Chem.* **2004**, *25*, 1157–1174.
- (39) Chelli, R.; Procacci, P.; Cardini, G.; Califano, S. *PCCP Phys. Chem. Chem. Phys.* **1999**, *1*, 879–885.
- (40) Vosko, S.; Wilk, L.; Nusair, M. *Can. J. Phys.* **1980**, *58*, 1200–1211.
- (41) Lee, C.; Yang, W.; Parr, R. *Phys. Rev. B* **1988**, *37*, 785–789.
- (42) Becke, A. *J. Chem. Phys.* **1993**, *98*, 5648–5652.
- (43) Stephens, P.; Devlin, F.; Chabalowski, C.; Frisch, M. *J. Phys. Chem.* **1994**, *98*, 11623–11627.
- (44) Frisch, M. J.; Trucks, G. W.; Schlegel, H. B.; Scuseria, G. E.; Robb, M. A.; Cheeseman, J. R.; Montgomery, J. A.; Vreven, T.; Kudin, K. N.; Burant, J. C.; et al. *Gaussian 03*, revision D.02; 2003.
- (45) Himo, F.; Siegbahn, P. *Chem. Rev.* **2003**, *103*, 2421–2456.
- (46) Cossi, M.; Rega, N.; Scalmani, G.; Barone, V. *J. Comput. Chem.* **2003**, *24*, 669–681.
- (47) Peng, C.; Schlegel, H. *Isr. J. Chem.* **1993**, *33*, 449–454.
- (48) Liao, R.-Z.; Yu, J.-G.; Himo, F. *J. Chem. Theory Comput.* **2011**, *7*, 1494–1501.
- (49) Himo, F. *Biochim. Biophys. Acta* **2005**, *1707* (1), 24–33.

- (50) Nordlund, P.; Reichard, P. *Annu. Rev. Biochem.* **2006**, *75*, 681–706.
- (51) Cho, K.; Himo, F.; Graslund, A.; Siegbahn, P. *J. Phys. Chem. B* **2001**, *105*, 6445–6452.
- (52) Cho, K.; Pelmenschikov, V.; Graslund, A.; Siegbahn, P. *J. Phys. Chem. B* **2004**, *108*, 2056–2065.
- (53) Smith, D.; Golding, B.; Radom, L. *J. Am. Chem. Soc.* **2001**, *123*, 1664–1675.
- (54) Kamachi, T.; Toraya, T.; Yoshizawa, K. *J. Am. Chem. Soc.* **2004**, *126*, 16207–16216.
- (55) Kamachi, T.; Toraya, T.; Yoshizawa, K. *Chem.—Eur. J.* **2007**, *13*, 7864–7873.
- (56) Kawata, M.; Kinoshita, K.; Takahashi, S.; Ogura, K.; Komoto, N.; Yamanishi, M.; Tobimatsu, T.; Toraya, T. *J. Biol. Chem.* **2006**, *281*, 18327–18334.
- (57) Kinoshita, K.; Kawata, M.; Ogura, K.-i.; Yamasaki, A.; Watanabe, T.; Komoto, N.; Hieda, N.; Yamanishi, M.; Tobimatsu, T.; Toraya, T. *Biochemistry* **2008**, *47*, 3162–3173.
- (58) Retey, J.; A, U.; Seibl, J.; Arigoni, D. *Experientia* **1966**, *22*, 502.